Journal of Water Process Engineering 63 (2024) 105518

Contents lists available at ScienceDirect

Journal of Water Process Engineering

journal homepage: www.elsevier.com/locate/jwpe

UVC-LED assisted photo-Fenton/peroxydisulfate processes for microcontaminant and bacteria removal in a continuous flow reactor according to EU 2020/741

T.B. Benzaquén [a], N. Pichel [b,c,1], P. Soriano-Molina [b,c,*], J.L. Casas López [b,c], G. Li Puma [d], J.A. Sánchez Pérez [b,c,*]

[a] Centro de Investigación y Tecnología Química (CITeQ), UTN-CONICET, Maestro Marcelo López esq. Cruz Roja Argentina, 5016ZAA Córdoba, Argentina
[b] Solar Energy Research Centre (CIESOL), Joint Centre University of Almeria-CIEMAT, Carretera de Sacramento s/n, 04120 Almeria, Spain
[c] Chemical Engineering Department, University of Almería, Ctra. de Sacramento s/n, Almería 04120, Spain
[d] Environmental Nanocatalysis & Photoreaction Engineering, Department of Engineering, University of Palermo (UNIPA), Palermo 90128, Italy

ARTICLE INFO

Editor: Akeem Oladipo

Keywords:
Reclaimed water
Advanced oxidation process
Escherichia coli
Clostridium perfringens
Micropollutant

ABSTRACT

Bacteria inactivation (*Escherichia coli* (*E. coli*), total coliforms, *Clostridium perfringens* (*C. perfringens*)) and simultaneous removal of ubiquitous microcontaminants in actual municipal wastewater treatment plant secondary effluents was investigated at neutral pH using the UVC-LED assisted photo-Fenton reaction system operated in continuous flow. *E. coli* concentration $\leq$ 10 CFU/100 mL and 38 % microcontaminant removal was achieved in the reaction system at a hydraulic residence time of 30 min. UVC light alone and UVC light combined with an oxidant source (hydrogen peroxide, H_2O_2, or peroxydisulfate, $S_2O_8^{2-}$) were found to have a predominant effect on disinfection, meeting the EU 2020/741 validation ($\geq$5 $\log_{10}$ reduction) and monitoring ($\leq$10 CFU/100 mL) targets for both *E. coli* and *C. perfringens* after 30 min of treatment in batch mode. However, in the presence of either 0.05 or 0.1 mM of ferric nitrilotriacetate (Fe^{3+}-NTA) the bacteria inactivation kinetics decreased due to reduced UVC light penetration along the water depth. In contrast, microcontaminant removal was accelerated using 0.05 or 0.1 mM of Fe^{3+}-NTA and 1.47 mM H_2O_2. Overall, the results revealed that the treatment conditions favouring microcontaminant removal hindered disinfection and vice versa, and that the disinfection levels of *C. perfringens* ($\leq 10^2$ CFU/100 mL) reached in the batch mode experiments could not be attained under the continuous flow regime. This points out the need of performing disinfection experiments under continuous flow operation, as shown in the present study to determine the disinfection performance of UVC-LED assisted photo-Fenton reaction systems.

1. Introduction

Under the effects of climate change, wastewater reclamation and reuse has become essential for the management of traditional water sources tackling water scarcity and security. Since June 2023, the European Union regulation 2020/741 regarding the minimum requirements for the reuse of water [1] has been in force. This regulation sets the quality of reclaimed water, in terms of disinfection limits, as a function of its intended use and irrigation method. It also includes a water reuse risk management plan to promote the identification and assessment of potentially dangerous agents, such as contaminants of emerging concern (CECs), which have yet to be regulated in the European Union.

Within this context, some of the challenges posed by current legislation include new plant upgrades to most municipal wastewater treatment plants (MWTPs) comprising the efficient management of tertiary treatments processes to guarantee compliance with the increasingly restrictive regulation for water reuse. This involves avoiding the formation of hazardous subproducts and removing microcontaminants, which is not possible with conventional chlorination treatment. Among different tertiary treatment options, advanced oxidation processes (AOPs) have long been studied and proposed as highly effective methods

* Corresponding authors at: Chemical Engineering Department, University of Almería, Ctra. de Sacramento s/n, Almería 04120, Spain.
E-mail addresses: psm727@ual.es (P. Soriano-Molina), jsanchez@ual.es (J.A.S. Pérez).
[1] Currently at School of Experimental Sciences and Technology, Rey Juan Carlos University, c/Tulipán s/n, 28933 Móstoles, Spain.

https://doi.org/10.1016/j.jwpe.2024.105518
Received 11 March 2024; Received in revised form 10 May 2024; Accepted 17 May 2024
Available online 22 May 2024

to inactivate resilient microorganisms and degrade CECs [2–5].

One of the most common AOPs for wastewater treatment is the photo-Fenton process, which generates hydroxyl radicals ($HO^{\bullet}$) with high oxidative potential by homogeneous and heterogeneous photocatalysis using iron (Fe^{2+}/Fe^{3+}), UV − vis light, and hydrogen peroxide (H_2O_2). The photo-Fenton process can be operated at neutral pH by using iron chelating complexes [6–8], such as nitrilotriacetic acid (NTA) which has proved to be a cost-effective chelating agent over the alternatives (ethylenediaminetetraacetic acid (EDTA), ethylenediamine-N, N′-disuccinic acid (EDDS), citric acid, among others). Previous works point out the high biodegradability of this compound and its lower toxicity risk for aquatic organisms in comparison with other chelating agents such as EDDS [9,10]. However, in-depth research on the toxicity of residual Fe^{3+}-NTA along with the degradation by-products of NTA after its use in the photo-Fenton process is required to evaluate the suitability of this compound for large-scale application.

Alternative sulfate-radical-based advanced oxidation processes (SR-AOPs) utilizing peroxymonosulfate (PMS) or peroxydisulfate (PDS) instead of H_2O_2 have also been proposed as effective processes for treating the degradation of refractory pollutants and disinfection of resistant microorganisms [11–13]. Among these SR-AOPs, the use of PDS has been widely studied due to the relatively long lifetime of the sulfate radicals ($SO_4^{\bullet-}$) generated [14], and operation under neutral pH [15].

Both photo-Fenton and SR-AOPs are also photo-controlled processes activated by UV and natural light, which can be replaced by the low-energy artificial light of LEDs [16,17]. Despite UVC-LEDs have been applied for drinking water disinfection [18–20], several studies have demonstrated the effectiveness of LEDs and AOPs for microcontaminant removal [21–23]. In this regard, it is worth mentioning that photo-Fenton and SR-AOPs could be competitive with ozone-based AOPs, since these processes involves lower operating costs related to equipment investment and energy consumption.

However, few studies have focused on simultaneous water decontamination and disinfection by UVC-LED driven systems for water reclamation applications, and those addressing it [23,24] have not taken into consideration UVC-resistant microorganisms included in the new European regulation for water reuse. A previous author's work addressed the comparison of UVC-LED/H_2O_2 and UVC-LED/$S_2O_8^{2-}$ processes (278 nm, 2 W/m^2 UVC irradiance) in a synthetic MWTP secondary effluent using a reference strain and a model microcontaminant [24]. However, as far as the authors know, there are no studies dealing with the use of this technology for the degradation of CECs contained in actual MWTP secondary effluents. In addition, there are no studies on simultaneous wastewater disinfection and microcontaminant degradation by UVC-LED processes in continuous flow.

Under a more realistic scenario, the main objective of this study was to evaluate the performance of a UVC-LED assisted photo-Fenton system operated in continuous flow mode, for simultaneous bacteria inactivation and microcontaminant removal, in MWTP secondary effluents. The effect of two oxidant sources (hydrogen peroxide, H_2O_2, and peroxydisulfate, $S_2O_8^{2-}$) combined with ferric nitrilotriacetate (Fe^{3+}-NTA) on acetamiprid (ACTM), *E. coli*, total coliforms (TC) and *C. perfringens* removal was initially studied in batch mode operation to determine the most effective treatment method. In addition, the feasibility of the UVC-LED assisted photo-Fenton system was studied in continuous flow mode operation, to demonstrate its applicability as a tertiary treatment process for the removal of CECs and the simultaneous inactivation of the new microbiological indicators set by the European regulation for the safe reuse of reclaimed water [1]. Thus, this work represents a promising and cutting-edge technological solution in the field of wastewater treatment.

2. Materials and methods

Information related to chemical reagents and analytical determinations is displayed as Supplementary Material (Appendix A1).

2.1. Water matrix characterization

The experiments were carried out with actual secondary effluents collected from the municipal wastewater treatment plant (MWTP) "El Toyo", located in the municipality of Almeria (Andalusia, Spain). The effluents were stored in a fridge (4 °C) and used for experimentation within the following two days. The experiments in batch mode were carried out using the effluents spiked with 50 μg/L of ACTM, as a model microcontaminant representing the total concentration of microcontaminants typically detected in secondary effluents. This is a recalcitrant pesticide included in the Watch List of Substances for European Union-wide monitoring reported in Decision 2018/840/EU [25]. Conversely, in the continuous flow experiments, the actual ubiquitous concentration of CECs present in the MWTP effluent was monitored without spiking of further microcontaminants.

Table 1 shows the average composition values of MWTP secondary effluents used during the experimentation. In previous investigations [7,8], the secondary effluents were pre-treated with sulfuric acid to reduce the concentration of inorganic carbon (IC) to a value close to 15 mg/L, as HCO_3^-/CO_3^{2-} ions act as scavengers of hydroxyl radicals [26]. Note that, in this work, experiments were carried out without any pre-treatment.

2.2. UVC-LED system experiments

Experiments were performed in a laboratory-scale UVC-LED photoreactor consisting of a UVC-LED system and a cylindrical polyvinyl chloride (PVC) reactor (Fig. 1). The UVC-LED system (Robotecno S.L, Spain), with an emission peak at 276 nm (range 260–320 nm) and maximum irradiance of 8.8 W/m^2 (Avantes AvaSpec-ULS2048–2), included a total of 25 diodes (5 lines connected in parallel, each one containing 5 diodes connected in series). The PVC reactor, with 1 L-capacity and 5-cm water depth, was placed horizontally beneath the UCV-LED system on a magnetic stirrer. Radiation distribution on the liquid surface was measured to check that the entire surface was irradiated (Supplementary Material, A2). Moreover, by actinometric measurements [27] (Supplementary Material, A3), the net radiative flux (q_w) (all diodes lit) on the reactor surface (177 cm^2) was determined to be 1.77×10^{-9} ($\pm$ 5.84×10^{-11}) E/cm^{2}s.

The first step involved a set of experiments performed in batch mode to determine the most effective operating conditions in continuous flow mode by varying: oxidant source ($H_2O_2/S_2O_8^{2-}$), reagent concentrations (oxidant source and Fe^{3+}-NTA) and hydraulic residence time (HRT). Accordingly, the effect of the combination of H_2O_2 or $S_2O_8^{2-}$ at an initial concentration of 1.47 mM, with three different initial concentrations of Fe^{3+}-NTA (0, 0.05 and 0.1 mM, Fe^{3+}:NTA molar ratio of 1:1) on bacteria and microcontaminants removal, was studied for 60 min. These reagent concentrations were selected based on a previous work conducted under

Table 1
Characterization of MWTP secondary effluent (El Toyo, Almeria, Spain).

Parameter	Unit	MWTP effluent
DOC	mg/L	7.03 (± 0.87)
IC	mg/L	55.2 (± 1.94)
Cl^-	mg/L	629 (± 77)
NO_2^-	mg/L	0.800 (± 0.040)
Br^-	mg/L	3.51 (± 0.17)
NO_3^-	mg/L	12.6 (± 1.5)
PO_4^{3-}	mg/L	9.11 (± 2.4)
SO_4^{2-}	mg/L	337 (± 28)
pH		7.51(± 0.10)
Conductivity	mS/cm	2.72 (± 0.12)
Turbidity	NTU	9.18 (± 4.21)

DOC: Dissolved Organic Carbon. IC Inorganic Carbon.

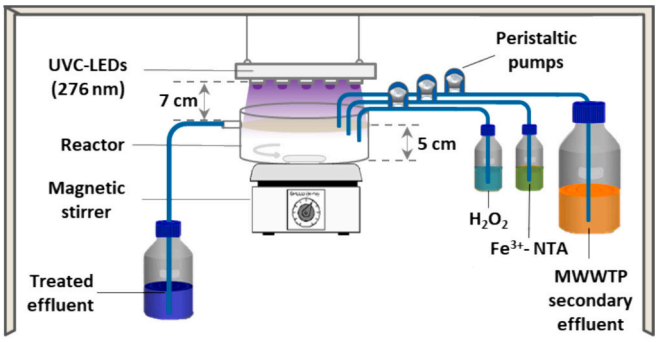

Fig. 1. Schematic representation of the experimental set-up in batch mode showing the UVC-LED system, water reactor, and magnetic stirrer layout; and MWTP secondary effluent and reagent inlets and treated water outlet connections when operating in continuous flow mode.

UVC-LED radiation [24]. Each experimental run began when the reactor was loaded with 1 L of MWTP secondary effluent (spiked with ACTM, 50 μg/L (2.24×10^{-4} mM)) and the reactor surface was shielded with a shutter located between the UVC-LED diodes and the liquid surface, to avoid radiation from entering. After that, the oxidant source (H_2O_2 or $S_2O_8^{2-}$) and Fe^{3+}-NTA were added and the reactor was immediately uncovered to start the photo-Fenton experiments (reaction time equal to zero).

Once the optimal operating conditions had been determined, the reactor was operated in continuous flow mode. Tests initially started in batch mode for 30 min, following the procedure described in a previous study [7] to ensure that the water contained in the reactor was not contaminated before starting the continuous flow operation. The wastewater and reactant supply pumps were subsequently turned on to initiate the continuous flow operation (one pass through the reactor). The treated water left the reactor through an overflow and was collected in a container. The hydraulic residence time (HRT) and reagent concentrations were set based on the results obtained in the batch operation. The measured pH and temperature of the effluent were around 7.2 ± 0.3 and 21 ± 1 °C, respectively, and experimentally verified to have remained almost constant throughout the runs performed. A sample from the RPR effluent was kept at room temperature for 24 h to assess regrowth of all indicators: *E. coli*, total coliforms and *C. perfringens*.

2.3. Bacteria enumeration

Naturally occurring *Escherichia coli*, total coliform and *Clostridium perfringens* were used as microbial indicators according to the EU 2020/741 regulation on minimum requirements for water reuse [1]. The membrane filtration technique was employed for the detection and enumeration of bacteria concentration with a detection limit (DL) of 1 CFU/100 mL. Samples were filtered through cellulose nitrate filters and then transferred to petri dishes with the suitable growth medium. Chromocult Coliform Agar (Merk) was used for *E. coli* and total coliforms determination. Petri dishes were incubated at 36 ± 2 °C for 21 ± 3 h. Dark blue to violet colonies were enumerated as *E. coli*, while salmon-pink to red colonies were enumerated as other coliforms [28]. The sum of both *E. coli* and other coliforms colonies corresponded to total coliforms. m-CP Agar Base (Scharlau) with m-CP Selective Supplement (Scharlau) was used for *C. perfringens*. Petri dishes were incubated anaerobically at 44 ± 1 °C for 21 ± 3 h. Colonies changing from yellow to pink colour when exposed to ammonium vapours were enumerated as *C. perfringens* [29].

The disinfection efficiency of the target microorganisms was calculated as follow (Eq. (1)):

$$\mathrm{LRV} = log_{10}N_0 - log_{10}\mathrm{N_t} = log_{10}\left(\mathrm{N_0}/\mathrm{N_t}\right) \quad (1)$$

where LRV represents the $\log_{10}$ reduction value obtained after a specific treatment time, N_0 is the microorganism concentration (CFU/100 mL) at the initial time, and N_t stands for the microorganism concentration (CFU/100 mL) at time t. In addition, inactivation kinetic data were described by the Chick-Watson linear model [30]. The inactivation kinetic was assessed by observing microorganism inactivation at different experimental conditions as a function of the elapsed time of treatment (Eq. (2)):

$$log_{10}\left(\mathrm{N_t}/\mathrm{N_0}\right) = -kt \quad (2)$$

where N_0 is the initial microorganism concentration, N_t the concentration of microorganisms (CFU/mL) at the treatment time t (min) and k the inactivation rate (1/min).

2.4. Determination of the UVC dose

The UVC-LED system irradiance was corrected to calculate the average irradiance in the water sample for each experimental condition as described by Bolton and Linden [31] (Eqs. (3)–(6)):

$$\mathrm{I_c} = \mathrm{E_0} \times \mathrm{F_R} \times \mathrm{F_P} \times \mathrm{F_W} \times \mathrm{F_D} \quad (3)$$

$$\mathrm{F_P} = \frac{\sum_{i=1}^{n} E_{m,i}/E_{m,C}}{\mathrm{n}} \quad (4)$$

$$\mathrm{F_W} = \frac{1\text{–}10^{-\mathrm{al}}}{\mathrm{a} \bullet \mathrm{l} \bullet ln(10)} \quad (5)$$

$$\mathrm{F_D} = \frac{\mathrm{L}}{(\mathrm{L}+\mathrm{l})} \quad (6)$$

where I_c is the corrected irradiance (mW/cm^2), E_0 the irradiance reading of the spectroradiometer at the centre point of the reactor surface (mW/cm^2), F_R the reflection factor that takes into account the reflection at the water/air interface (0.975), F_P the petri factor that takes into account for the horizontal divergence (0.734), $E_{m,C}$ (mJ/cm^2·s) the incident irradiance at the centre of the sample surface, $E_{m,i}$ (mJ/cm^2·s) the incident irradiance at the sample surface at point i (measured every 5 mm), F_W (−) the water factor, a (1/cm) the absorption coefficient, 1 (cm) the vertical path length of the sample, F_D (−) the divergence factor, and L (cm) the distance between the surface of the sample and the UVC system. The I_C was calculated for each experimental condition and used to calculate the effective applied UVC_{276} dose.

2.5. Energy and reagent cost

A cost analysis (at laboratory scale), focusing on the energy consumption of the UVC-LED system, pumps and reagents, was carried out to estimate the cost of treated water in Euro (€) per m^3. A digital multimeter (PeakTech 3445) was used to determine the power of the UVC-LED panel. The amperage of each line made of 5 diodes connected in series was about 100 mA, with a total of 500 mA for the 5 lines connected in parallel and a voltage of 40 V. The power of the 20-W UVC-LED direct current (DC) panel was calculated by multiplying the measured voltage and associated current. The electrical energy consumption and associated cost was calculated multiplying the power of the LED panel by the required water treatment time. Additional energy cost includes that from a 1-W pump for the effluent pumping plus two 5 W pumps for reagent dosing. An electricity price of 0.131 €/kWh (business rate, June 2022, Spain) (Global Petrol Prices) was considered. Reagent costs for industrial-grade prices were: 0.71 €/kg $Fe_2(SO_4)_3{\cdot}H_2O$ (75 %, *w*/w), 0.95 €/kg NTA (99 % w/w), 0.1 €/L H_2SO_4 (98 % w/w), and 0.45 €/L H_2O_2 (33 % *w*/*v*) [32].

3. Results

3.1. Batch mode operation

E. coli, total coliforms and *C. perfringens* were detected in the MWTP effluent with initial concentrations of 10^3–10^4, 10^4–10^6 and 10^2–10^3 CFU/100 mL, respectively. Inactivation kinetics at different tested experimental conditions (Table 2) are shown in Fig. 2 (vs. UV dose) and in Fig. A4 of Supplementary Material (vs. exposure time). The relationship between *E. coli* LRVs and treatment time followed a linear trend as described by the Chick-Watson inactivation model, showing neither shouldering nor tailing effect. *E. coli* reached the DL after a maximum of 4 min of treatment (with UVC_{276} doses ranging from 20 mJ/cm^2 to 88 mJ/cm^2), regardless of the experimental conditions, achieving a reduction of 4 (± 0.56) log-units within the tertiary treatment process. However, it was observed that the oxidant source (H_2O_2 and $S_2O_8^{2-}$) and the concentration of Fe^{3+}-NTA used affected the inactivation rate constant to a different extent. Higher inactivation rates were found in those experiments combining UVC light and one oxidant (H_2O_2 or $S_2O_8^{2-}$) or when the system was operated by only UVC light (Table 2). In terms of oxidants, $S_2O_8^{2-}$ showed a higher disinfection activity than H_2O_2, both in the absence and in combination with Fe^{3+}-NTA (Table 2). In the presence of Fe^{3+}-NTA, the bacteria inactivation kinetics decreased as the concentration of Fe^{3+}-NTA was increased up to 0.1 mM, indicating that Fe^{3+}-NTA shielded UVC light and its propagation through the reactor depth. Note that the estimated optical thickness, τ (Supplementary Material, Eq. A5.1), increased from 3.1 to 6.2 when doubling Fe^{3+}-NTA concentration.

Inactivation of total coliforms is better represented by a biphasic inactivation curve with a fast inactivation rate fitting a first order decay model at low doses (10–35 mJ/cm^2), followed by a slower inactivation rate at higher doses (35–1350 mJ/cm^2), which consisted of a shoulder and then a tail (Fig. 2b). The value of *k* was obtained from the slope in the linear portion of the curve. TC inactivation was faster in the presence of UVC light and one oxidant source, or only in the presence of UVC light (Fig. 2b, Table 2). In the presence of H_2O_2, the addition of iron slowed down the disinfection process by 7 % at 0.05 mM Fe^{3+}-NTA increasing to a 29 % at 0.01 mM at Fe^{3+}-NTA. When using $S_2O_8^{2-}$ as the oxidant source, the inactivation rate decreased 11 % and 44 %, respectively (Table 2). In addition, it was observed that the combination of UVC light/H_2O_2/Fe^{3+}-NTA showed better results than UVC light/$S_2O_8^{2-}$/Fe^{3+}-NTA (Table 2). At low initial concentrations (10^4 CFU/100 mL), total coliforms reached the DL in all tested conditions after 60 min of treatment, except for the combination of UVC light/$S_2O_8^{2-}$/0.1 mM Fe^{3+}-NTA, with an average LRV of 4.7 (± 0.37).

Concerning the simultaneous removal of the spiked ACTM micro-contaminant (Fig. 3), in all cases, a pseudo-first order trend was adopted to represent ACTM decay. The rate constants, calculated from the slope in the linear part of the curve (corresponding to the first 15 min of the reaction), are shown in Table 2. As can be seen, UVC alone was not effective in the degradation of ACTM, reaching only a removal of 17 % after 60 min. Using $S_2O_8^{2-}$ as an alternative oxidant for the photo-Fenton reaction, a low removal rate was found in experiments combining UVC

Table 2
Inactivation rate constant *k* for *E. coli*, total coliforms and *C. perfringens* and removal rate constant *k* of ACTM, and R^2-coefficient for the experimental conditions tested in the UCV-LED assisted photo-Fenton system.

E. coli	k ± SD 1/min	R^2
UVC light	3.804 ± 0.105	0.999
UVC light + H_2O_2	3.040 ± 0.438	0.998
UVC light + $S_2O_8^{2-}$	6.278 ± 2.676	0.973
UVC light +0.05 mM Fe^{3+}-NTA + H_2O_2	1.456 ± 0.467	0.984
UVC light +0.1 mM Fe^{3+}-NTA + H_2O_2	0.888 ± 0.213	0.980
UVC light +0.05 mM Fe^{3+}-NTA + $S_2O_8^{2-}$	1.591 ± 0.332	0.985
UVC light +0.1 mM Fe^{3+}-NTA + $S_2O_8^{2-}$	1.304 ± 0.437	0.955
Total coliforms		
UVC light	1.653 ± 0.052	0.968
UVC light + H_2O_2	1.796 ± 0.392	0.969
UVC light + $S_2O_8^{2-}$	1.890 ± 0.294	0.909
UVC light +0.05 mM Fe^{3+}-NTA + H_2O_2	1.541 ± 0.068	0.964
UVC light +0.1 mM Fe^{3+}-NTA + H_2O_2	1.177 ± 0.040	0.992
UVC light +0.05 mM Fe^{3+}-NTA + $S_2O_8^{2-}$	1.473 ± 0.022	0.992
UVC light +0.1 mM Fe^{3+}-NTA + $S_2O_8^{2-}$	0.934 ± 0.163	0.992
C. perfringens		
UVC light +0.05 mM Fe^{3+}-NTA + H_2O_2	0.090 ± 0.014	0.983
UVC light +0.1 mM Fe^{3+}-NTA + H_2O_2	0.038 ± 0.012	0.970
ACTM		
UVC light	0.0068 ± 0.0001	0.918
UVC light + H_2O_2	0.0104 ± 0.0023	0.998
UVC light +0.05 mM Fe^{3+}-NTA + H_2O_2	0.0129 ± 0.0033	0.994
UVC light +0.1 mM Fe^{3+}-NTA + H_2O_2	0.0370 ± 0.0010	0.995
UVC light + $S_2O_8^{2-}$	0.0051 ± 0.0001	0.945
UVC light +0.05 mM Fe^{3+}-NTA + $S_2O_8^{2-}$	0.0064 ± 0.0006	0.985
UVC light +0.1 mM Fe^{3+}-NTA + $S_2O_8^{2-}$	0.0066 ± 0.0014	0.962

SD: standard deviation.

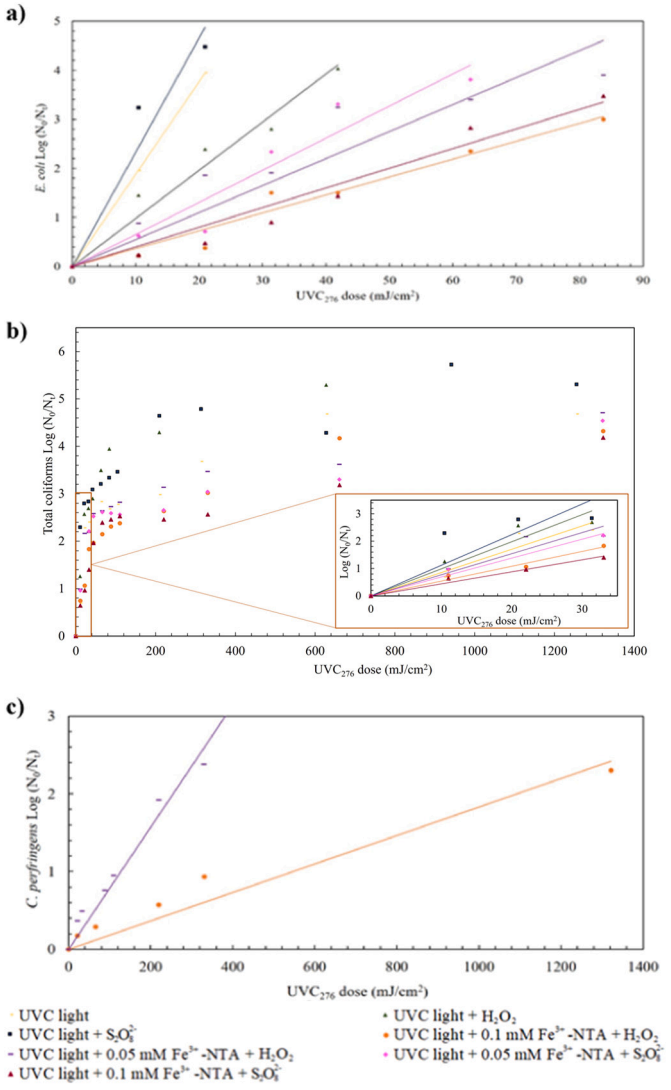

Fig. 2. *E. coli*, total coliforms and *C. perfringens* inactivation kinetics (dots) determined in the UVC-LED assisted photo-Fenton reactor combining UVC light, Fe^{3+}-NTA (0.05 and 0.1 mM) and H_2O_2 or $S_2O_8^{2-}$ (1.47 mM); and Chick-Watson linear model fitting (lines).

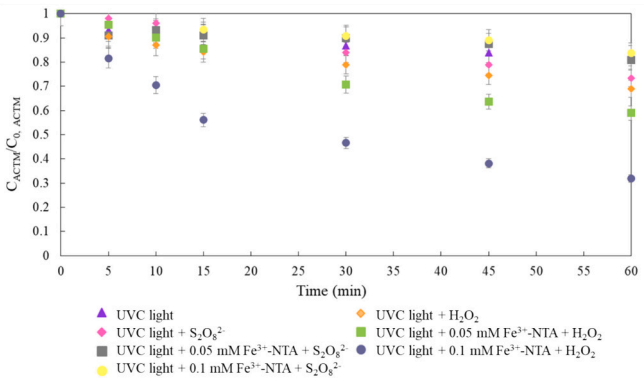

Fig. 3. ACTM removal profiles in the UVC-LED assisted photo-Fenton reactor combining UVC light, H_2O_2 or $S_2O_8^{2-}$ (1.47 mM) and Fe^{3+}-NTA (0.05 and 0.1 mM).

light and $S_2O_8^{2-}$, not being able to remove >27 % of ACTM after 60 min of treatment and not showing improvement even in the presence of an iron source (Table 2). In contrast, with the traditional oxidant of the photo-Fenton reaction (H_2O_2), higher degradation efficiencies were obtained. The presence of this oxidant in the reaction bulk (UVC light + H_2O_2) enhanced the rate of ACTM removal by 1.5 times (Table 2). However, only a 31 % elimination was achieved after 1 h of reaction. The addition of 0.05 mM and 0.1 mM of Fe^{3+}-NTA (UVC light + Fe^{3+}-NTA + H_2O_2) accelerated microcontaminant degradation by 1.2 and 3.6 times, respectively, giving rise to 40 % and 68 % ACTM removal after 60 min of the reaction. Considering these removal percentages, Fe^{3+}-NTA efficiencies, estimated as the number of moles of microcontaminant removed per number of moles of Fe^{3+}-NTA and unit of time [33], were 0.0018 and 0.0015, with 0.05 and 0.1 mM of Fe^{3+}-NTA, respectively. These efficiencies are characteristic of microcontaminant removal because the iron concentration is typically 3–4 orders of magnitude higher than microcontaminant concentration. In addition, it is important to mention that after Fe^{3+}-NTA photo-decomposition iron precipitates, leading to the formation of iron hydroxide.

As for the reagents, only 10 % of the initial H_2O_2 concentration was consumed after 60 min under UVC irradiation, whereas the presence of iron significantly accelerated the oxidant conversion. Pseudo-first order constants increased from 0.007 (± 0.0016) 1/min ($r^2 = 0.977$) to 0.0175 (± 0.0001) 1/min ($r^2 = 0.937$), when doubling the Fe^{3+}-NTA concentration from 0.05 mM to 0.1 mM, respectively, leading to 19.43 % and 44.54 % of H_2O_2 consumption. The consumption of $S_2O_8^{2-}$, for all the conditions tested, was insignificant over the experimental time and it could not be quantified by the analytical method. Concerning the total dissolved iron profiles, in all cases the complex totally decomposed after 60 min of the reaction. With 0.1 mM Fe^{3+}-NTA, the loss of iron in solution was faster in the presence of H_2O_2 than with $S_2O_8^{2-}$. In general, the loss of iron in solution, and therefore, of photodecomposition of the complex, was greater in the tests with H_2O_2 than with $S_2O_8^{2-}$, in accordance with the higher rate of oxidant consumption and microcontaminant degradation.

Due to the poor ACTM removal results obtained with $S_2O_8^{2-}$ as an oxidant source, its use was excluded. As such, inactivation of *C. perfringens* (well known for its resilience to UVC radiation) was evaluated with H_2O_2 (1.47 mM) at 0.05 and 0.1 mM Fe^{3+}-NTA (Fig. 2c). With a delivered UVC_{276} dose of 660 mJ/cm^2, the DL was reached after 30 min of treatment when working at 0.05 mM Fe^{3+}-NTA (3 ± 0.42 LRV). However, using a higher Fe^{3+}-NTA concentration (0.1 mM), an average of 80 CFU/100 mL remained after 60 min, not reaching the DL (UVC_{276} dose 1322 mJ/cm^2) (2.3 ± 0.32 LRV). Once again, higher Fe^{3+}-NTA concentrations translated into lower inactivation rates (Fig. 2c, Table 2), with 60 % inactivation reduction at 0.1 mM Fe^{3+}-NTA vs 0.05 mM Fe^{3+}-NTA.

The results of this comparative study under batch operation, suggested a compromise in the operating conditions to achieve effective simultaneous disinfection and decontamination of the MWTP effluent. Thus, the UVC-LED assisted photo-Fenton reactor in continuous flow mode was operated using the following conditions: UVC light/0.735 mM H_2O_2/0.05 mM Fe^{3+}-NTA, UVC light/1.47 mM H_2O_2/0.1 mM Fe^{3+}-NTA, and only UVC light as control, working at 30 min HRT.

3.2. Continuous flow operation

The reactor was initially operated in batch mode for 30 min, and then in continuous flow mode for 180 min. The hydrogen peroxide, and total dissolved iron profiles, are shown in Fig. 4. During the batch stage, an expected drop in reactant concentrations was observed. Once the feed pumps for reagents and wastewater were switched on there was a transitional time until a steady state was reached. The steady-state concentrations were 0.018 (±0.002) mM and 0.0394 (±0.009) mM of total dissolved iron for the UVC-LED/0.735 mM H_2O_2/0.05 mM Fe^{3+}-NTA and UVC-LED/1.47 mM H_2O_2/0.1 mM Fe^{3+}-NTA processes, respectively, at the HRT tested. Similar results in terms of H_2O_2 consumption were obtained with both processes, reaching a steady-state concentration of 0.58 (±0.017) mM and 1.05 (±0.092) mM, for UVC-LED/0.05 mM Fe^{3+}-NTA/0.735 mM H_2O_2 and UVC-LED/0.1 mM Fe^{3+}-NTA/1.47 mM H_2O_2 processes, respectively. As shown in Fig. 4, dimensionless profiles of H_2O_2 and dissolved iron overlapped when doubling both concentrations simultaneously. This is in line with first order kinetics (Eq. (7)), where k is constant and the dimensionless concentration profile does not change.

$$ln\left(C_t/C_0\right) = -kt \tag{7}$$

The bacteria inactivation and the sum of CECs degradation profiles, for continuous flow operation are shown in Fig. 5. Initial bacteria concentrations in the secondary effluent were 10^3 CFU/100 mL for *E. coli*, 10^4 CFU/100 mL for TC and 10^2–10^3 CFU/100 mL for *C. perfringens*. Bacteria concentration reached steady state in <30 min. In batch operation, *E. coli* always reached the DL during the 30 min treatment time, regardless of the experimental conditions (Fig. 5a). The DL for total coliforms, as well as for *C. perfringens*, was not attained under the experimental conditions UVC light/1.47 mM H_2O_2/0.1 mM Fe^{3+}-NTA, with an average final concentration of 10 CFU/100 mL for both indicators (Fig. 5b-c). During the continuous flow operation, *E. coli,* TC and *C. perfringens* concentration in the photoreactor declined as the iron concentration increased (Table 3), only attaining the highest level of inactivation when the reactor was run under UVC-LED light. *E. coli* load in the photoreactor effluent was ≤10 CFU/100 mL, except for the UVC light/1.47 mM H_2O_2/0.1 mM Fe^{3+}-NTA condition, which returned an average concentration of 30 (±5) CFU/100 mL. None of the indicator microorganisms reached the DL in continuous flow operation.

The number of CEC compounds detected at steady state in the reactor effluent varied according to the treatment methods and experimental conditions and ranged from 51 to 71. These compounds (Table 4) were mainly pharmaceuticals (such as anti-inflammatories, analgesics, antibiotics, cardiovascular and psychiatric drugs) and pesticides (such as acetamiprid and imidacloprid).

At the end of the batch stage, the CEC concentration had decreased in all cases, the CEC removal rate being double in the experiment carried out with UVC-LED/1.47 mM H_2O_2/0.1mMFe^{3+}-NTA (Fig. 5d), with respect to the other two conditions (UVC light alone and UVC-LED/0.05 mM Fe^{3+}-NTA/0.735 mM H_2O_2). With UVC-LED/0.735 mM H_2O_2/0.05 mM Fe^{3+}-NTA, 42 % of the contaminants were degraded; and with UVC-LED/0.1 mM Fe^{3+}-NTA/1.47 mM H_2O_2 a removal percentage of 76 % was attained. For continuous flow operation, the CEC removal, reached steady stay in about 30 min and the steady state percentages were 24 %, 38 % and 63 %, for UVC-LED, UVC-LED/0.735 mM H_2O_2/0.05 mM

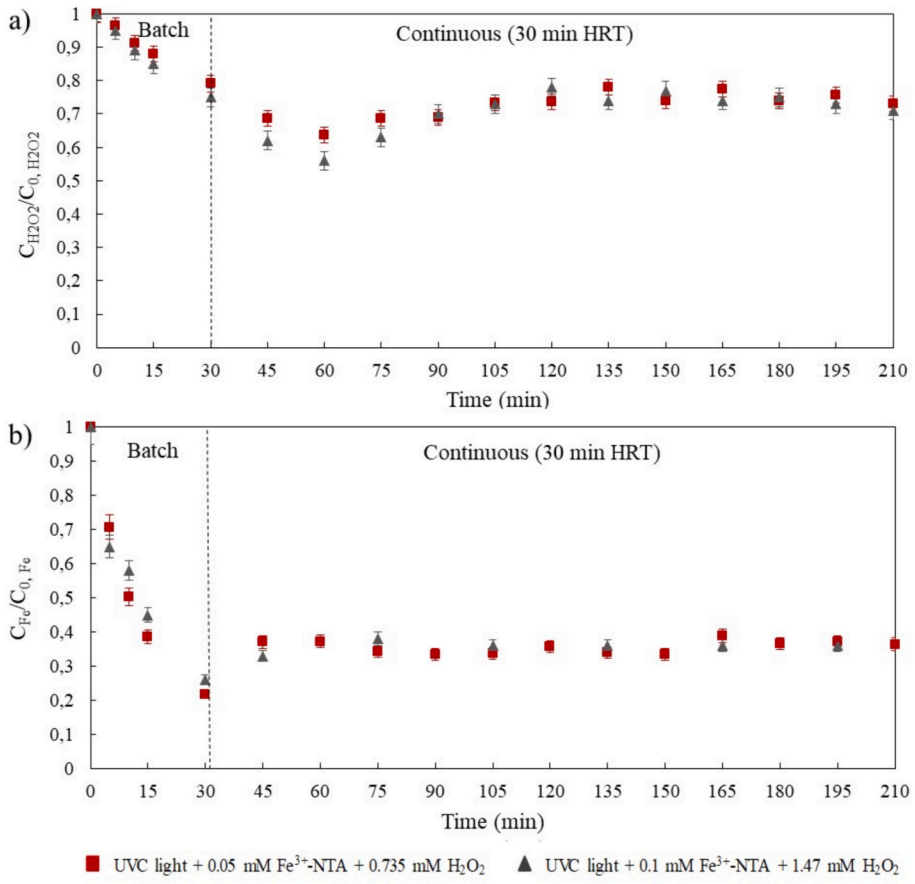

Fig. 4. a) H_2O_2 consumption and b) Dissolved iron by UVC-LED assisted photo-Fenton process operated in continuous flow.

Fe^{3+}-NTA and UVC-LED/1.47 mM H_2O_2/ 0.1 mM Fe^{3+}-NTA processes, respectively.

The degradation profiles of all compounds over time and the removal percentages of each effluent for each condition are shown in Supplementary Material, A6. The CECs were found in concentrations of the same order of magnitude in all the secondary effluents and some metabolites of dipyrone such as 4-aminoantipyrine (4-AA) and 4-formylaminoantipyrine (4-FAA), Lamotrigine, Oxypurinole, Sulpiride, Tramadol and *O*-desmethyltramadol were found with the highest initial concentrations.

Table 4 shows the initial loads and the percentage removal, after the period in batch mode and continuous mode, respectively, of the 10 pollutants with the highest load in the experiment with UVC/0.1 mM Fe^{3+}-NTA/1.47 mM H_2O_2.

The sum of the load of these most abundant compounds represented 72 % of the total load of CECs. As can be seen during the batch period, most of these pollutants exceeded 90 % removal in only 30 min. Moreover, during continuous mode, most of them reach degradations above 70 %. The oxypurinole compound showed the greatest load and resistance to degradation, reaching only 23 % degradation during the batch period and 14.1 % during the continuous period. In continuous operation, the presence of the highest concentration of iron increased the removal of CECs 2.6 times more than the condition with half the concentration of reagents, and 1.6 times compared to the absence of these reactants.

4. Discussion

This comparison study showed that the treatment conditions favouring disinfection hindered microcontaminant removal and vice versa. UVC light was found to be the predominant factor on disinfection. In this regard, average UVC_{276} absorbance in the testing samples increased from 0.182 (±0.007) in the absence of an iron source, to 0.451 (±0.04) at 0.05 mM of Fe^{3+}-NTA and to 0.600 (±0.02) at 0.1 mM Fe^{3+}-NTA. Thus, Fe^{3+}-NTA concentration which directly contributes to ultraviolet transmittance (UVT) at the UVC-LED emission peak (276 nm), greatly affects the inactivation rate constant. Radiation absorption by Fe^{3+}-NTA negatively influences the disinfection process by increasing light radiation absorbance at the emission peak of the UVC-LED system. Thus, the addition of Fe^{3+}-NTA hindered bacteria inactivation by reducing the UVC light delivered to the microorganisms. Indeed, the optimum optical thickness reported for photocatalytic systems, $\tau = 3$ [34], was obtained with 0.05 mM of Fe^{3+}-NTA, meaning that 95.8 % of the radiation in the reactor was absorbed by iron. This value was doubled with 0.1 mM of Fe^{3+}-NTA, pointing out that 99.8 % of the radiation was absorbed and hence there were no photons available for disinfection. In addition, it is worth mentioning that 79 % and 95 % of the incident UVC radiation was absorbed at a liquid depth of 2.5 cm with 0.05 mM and 0.1 mM of Fe^{3+}-NTA, respectively, as shown in Fig. A7 (Supplementary Material). These results agree with previous works, which indicated a 40–50 % reduction in bacteria and coliphages inactivation due to radiation absorption in the testing sample, negatively influencing the disinfection efficiency of advanced oxidation processes such as UV/H_2O_2, photo-Fenton and photocatalysis [35,36]. In actual MWTP secondary effluents, the hydroxyl radical-scavenger effect of reactive species such as ions and organic matter must also be considered. It negatively affects the inactivation process by inhibiting the oxidative attack, due to generated radicals lacking inherent selectivity towards pathogens. In addition, reactive species affect H_2O_2 consumption, which has been shown to reduce photo-Fenton degradation activity by half [37,38].

Results are also in accordance with those obtained by Miralles-

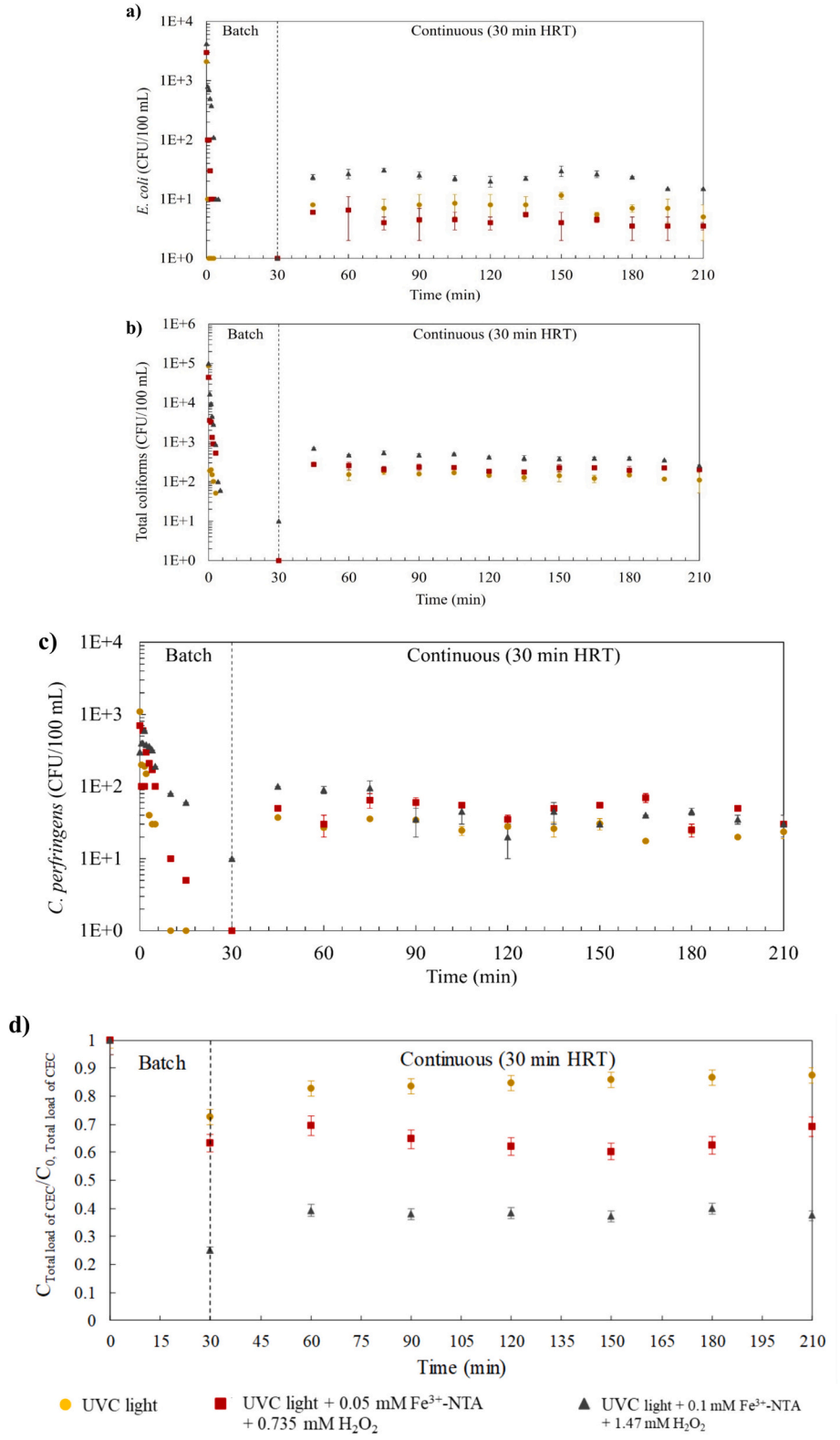

Fig. 5. a) *E. coli* inactivation, b) total coliforms inactivation, c) *C. perfringens* inactivation and d) CEC degradation; by UVC-LED assisted photo-Fenton process operated in continuous flow with the secondary effluent from 'El Toyo' WWTP (Almería, Spain).

Cuevas et al. [24] who investigated the UVC_{278}-LED assisted photo-Fenton process for simultaneous bacteria and microcontaminant removal and concluded that longer irradiation times are required to reach the DL (100 CFU/100 mL) when adding Fe^{3+}-NTA to the testing sample. However, unlike the results displayed here, UVC radiation was not found to have the predominant germicidal effect, getting faster inactivation rates when operating the system in combination with the photo-Fenton reaction (30 min) as opposed to only using UVC_{278} light (not reaching the DL after 60 min). This could be attributed to the matrix effect since synthetic water was used instead of real MWTP secondary

Table 3
E. coli, total coliforms and *C. perfringens* inactivation (showed as LRV) attained in continuous flow operation at the different testing conditions: UVC-LED light, UVC-LED/0.735 mM H_2O_2/0.05 mM Fe^{3+}-NTA and UVC-LED/1.47 mM H_2O_2/0.1 mM Fe^{3+}-NTA.

	E. coli	Total coliforms	*C. perfringens*
UVC-LED	2.5 (±0.102)	2.8 (±0.113)	2.8 (±0.095)
UVC-LED/0.735 mM H_2O_2/0.05 mM Fe^{3+}-NTA	2.7 (±0.085)	2.3 (±0.053)	1.2 (±0.149)
UVC-LED/1.47 mM H_2O_2/0.1 mM Fe^{3+}-NTA	2.3 (±0.096)	1.2 (±0.053)	0.8 (±0.221)

Table 4
Initial concentrations (ng/L) of the most relevant CECs detected in the MWTP effluent used.

Contaminant	Initial load	%Removal	
	ng/L	Batch	Continuous
4-AA	2414.2	98.7	95.4
4-AAA	1105.8	94.8	74.3
4-FAA	7800.0	100.0	97.6
Irbesartan	1374.7	98.9	78.7
Lamotrigine	1106.1	79.3	49.5
O-Desmethyltramadol	1667.9	94.6	70.6
O-Desmethylvenlafaxine	1555.5	96.7	69.3
Oxypurinole	10,073.6	23.2	15.9
Sulpiride	1141.0	82.7	54.1
Tramadol	1470.0	100.0	64.3
Other CECs[a]	11,442.1	88.7	70.3
Total load of CECs	**41,150.8**	**76.4**	**62.8**

[a] Sum of the concentrations of the rest of detected CECs.

effluent. This could benefit the photo-Fenton reaction as it favours a higher $HO^{\bullet}$ concentration and consequently a higher inactivation rate. It is important to remark that a cultured strain (*E. coli* K12), more sensitive than a wild strain, was used as a microbial indicator by Miralles-Cuevas et al. [24]. In López-Vinent et al. [39], longer treatment times (120 min) were necessary to achieve 4 LRV of naturally occurring *E. coli* and TC in a UVA-LED assisted photo-Fenton system, which could reassert the predominant role of UVC light over the photo-Fenton process on bacteria inactivation in real MWTP effluents. In contrast, despite the UVC-dose response for a wide range of microorganism using LEDs at different wavelengths being reported [18], there is lack of information about *C. perfringens*. Only Kamel et al. [40] studied inactivation of this pathogenic microorganism for MWTP secondary effluent reclamation using UVC-LED$_{279}$. This work showed shorter times (7 vs. 30 min) and lower doses (196 vs. 660 mJ/cm^2) to achieve the same log-reduction. This difference in results reasserts the negative effect of the iron source on disinfection, which could be also attributed to different experimental configurations, the liquid depth (0.7 vs. 5 cm) being more relevant. Clearly optimisation of the treatment system will be achieved by optimising reactant concentration and liquid depth to achieve optical thicknesses of about $\tau = 3$ [34]. At much higher values of optical thickness light distribution across the reactor is hindered and therefore bacteria disinfection is inhibited, while at much lower optical thicknesses bacteria disinfection is favoured and CEC removal is hindered.

Microcontaminant removal was favoured by the presence of Fe^{3+}-NTA and H_2O_2 in the system. Under UV radiation, this iron complex photoactivates giving rise to Fe^{2+} (R.1). This photodegradation involve a $HO^{\bullet}$ generation, and possibly the appearance of other less reactive radicals (R.2). When H_2O_2 is added, on the one hand the generated Fe^{2+} is oxidized giving rise to Fe^{3+} (Fenton reaction) and a stoichiometric amount of $HO^{\bullet}$; and on the other hand, the iron complex can react to generate additional Fe^{2+}, NTA free radical, hydroperoxide radical and hydroxyl radicals as well as hydroxyl anions (R.3) – (R.5), according to the following reaction mechanism [32]:

$$Fe^{3+} - NTA + h\nu \rightarrow Fe^{2+} + NTA^{\bullet} \quad (R.1)$$

$$NTA^{\bullet} + O_2 \rightarrow NTA_{OX} + O_2^{\bullet -} \quad (R.2)$$

$$Fe^{2+} + H_2O_2 \rightarrow Fe^{3+} + HO^{\bullet} + HO^{-} \quad (R.3)$$

$$Fe^{3+} - NTA + H_2O_2 \rightarrow Fe^{2+} - NTA + HO_2 + H^{+} \quad (R.4)$$

$$Fe^{2+} - NTA + H_2O_2 \rightarrow Fe^{3+} - NTA + HO^{\cdot} + HO^{-} \quad (R.5)$$

Increasing the concentration of the complex (limiting reagent) substantially accelerated the reaction rate, which indicates that the radiation absorption by Fe^{3+}-NTA positively influences the process. These findings agree with previous works indicating that the $HO^{\bullet}$ radical generation was enhanced by increasing the dosages of reagents, and with other studies which point out the importance of iron complexation for the production of reactive radicals in the Fenton reaction at neutral pH [38,41,42]. In addition, it is important to remark that, the molar absorptivity of Fe^{3+}-NTA complex at different wavelengths has also been reported by other authors [6,24,32], who all indicate that it increases at low wavelengths, and consequently the Fe^{3+}–NTA photodecomposition under UVC is higher than that obtained with other UV sources. Although there are many reactions and processes which work simultaneously during UVC photo-Fenton treatment at neutral pH, the main mechanisms involved in microcontaminant removal are stated to be those related to the generation of hydroxyl radicals which attack the recalcitrant molecules [43]. Comparing the results obtained in this study with those reported in a previous study conducted under solar radiation [44], disinfection times were significantly shortened (<5 min vs 120 min) due to the stronger bactericidal effect UVC-LED. However, similar microcontaminant degradation was attained after 30 min of the reaction (70 % - 80 %) due to it mainly depends on oxidation with the hydroxyl radicals. Consequently, the hydraulic residence time selected for the continuous flow operation of the UVC-LED system, based on the experimental obtained results from the batch mode operation in the first stage of this study, agrees with the value reported in a previous work on solar photo-Fenton with Fe^{3+}-NTA for microcontaminant removal [38].

UVC light or the combination of UVC light with $S_2O_8^{2-}$ or H_2O_2 were not efficient in the degradation of CECs, which suggests that the MWTP secondary effluents used are photolytically stable under UVC radiation (276 nm) and the oxidizing potentials of $S_2O_8^{2-}$ or H_2O_2 are not sufficient to degrade recalcitrant microcontaminants. The results point out that although persulfate radicals react selectively with organic compounds against hydroxyl radicals, which are non-selective [45], a higher concentration of oxidant and longer reaction time than in the photo-Fenton process are needed to remove the microcontaminants.

Concerning the system's applicability as a tertiary treatment according to EU 2020/741 [1], validation of tertiary treatment plants producing water with the highest quality requirements (Class A) must be performed considering the bacteria concentration in the raw water entering the MWTP [1]. Disinfection objectives are ≥5 log-units for *E. coli* and spore-forming sulfate-reducing bacteria, or disinfection below the DL when they do not have sufficient quantity to reach the required $\log_{10}$ reduction. In addition, *E. coli* concentration must be monitored frequently in reclaimed water intended for agricultural irrigation to ensure the water quality at the catchment point. Its concentration must be ≤10 CFU/100 mL for water quality class A, ≤10^2 CFU/100 mL for class B, ≤10^3 CFU/100 mL for class C and ≤10^4 CFU/100 mL for class D. *E. coli*, TC and *C. perfringens* were detected in the 'El Toyo' MWTP inlet with initial loads of 10^6, 10^7 and 10^5 CFU/100 mL, respectively. In batch mode, the disinfection levels obtained for the whole treatment process were ≥5 log-units for *E. coli* and *C. perfringens*, with an *E. coli* concentration ≤10 CFU/100 mL, meeting the EU 2020/741 disinfection targets, although *C. perfringens* did not attain ≥5 LRV when operating at 0.1 mM Fe^{3+}-NTA. In continuous flow operation, both disinfection targets were met for *E. coli* when working only with

UVC light and in the UVC light/0.735 mM H_2O_2/0.05 mM Fe^{3+}-NTA combination. *E. coli* concentration in the effluent photoreactor was >10 CFU/100 mL when working at UVC light/1.47 mM H_2O_2/0.1 mM Fe^{3+}-NTA. However, the validation target of ≥5 log-reduction was not attained for *C. perfringens* regardless of the experimental conditions when operating in continuous flow mode. It reached an average of 3.7 (±0.095) LRV when operating the system with only UVC light, decreasing to 3.5 (±0.146) LRV at UVC light/0.735 mM H_2O_2/0.05 mM Fe^{3+}-NTA and to 3.5 (±0.221) LRV at UVC light/1.47 mM H_2O_2/0.1 mM Fe^{3+}-NTA. In addition, no regrowth of any of the indicators was observed 24 h after treatment. In this regard, it is worth mentioning that the residual H_2O_2 concentration (in the range of 0.6–1.0 mM) would not pose any risk for water reuse in agricultural irrigation [46,47].

Finally, from a cost-effectiveness point of view, it is critical to perform a thorough study of all the interrelations between the aforementioned factors as part of the objectives, in order to achieve the optimum operating conditions. The energy cost of reclaimed water was estimated based on data obtained at laboratory-scale, although larger-scale data are required to produce more accurate results. Electric power consumption and cost calculations are shown in Supplementary Material, A8. To this end, the treatment time required to achieve both bacteria (according to EU 2020/741 regulation) and CEC removal targets, along with the electricity and reagent cost (€) per m^3, were considered. The energy cost of reclaimed water associated with the UVC-LED panel consumption was estimated at 1.31 €/m^3 (1.41 USD/m^3), the total operation cost (UVC-LEDs, pumps, and reagents) for both reagent concentration (0.735 mM H_2O_2/0.05 mM Fe^{3+}-NTA, 1.47 mM H_2O_2/0.1 mM Fe^{3+}-NTA) being 1.32 €/m^3 (1.43 USD/m^3). Thus, the electricity cost of the UVC-LED panel accounts for 99 % of the total costs. However, if compared with low-pressure (LP) mercury lamps (UVC_{254}), widely used as a UVC light source for disinfection, higher electricity consumption is required to reach the same disinfection levels. For comparison purposes, *E. coli* was used as the indicator bacterium, since being one of the most studied microorganisms in the literature, all the data needed to perform the calculations was available, which was not the case with *C. perfringens*. One study [48], using a 12 W LP mercury lamp, reported 4 LRV of *E. coli* after 2.8 min in 100 mL sample, which equates to 0.73 €/m^3 vs. the 0.17 €/m^3 required to achieve the same *E. coli* inactivation level with UVC_{276}-LED light (20 W UVC_{276}-LEDs, 4 min, 4 LRV and 1 L sample). As such, the use of LEDs led to a 4-fold reduction of electricity-induced costs. Furthermore, in addition to competitive energy costs, LEDs possess other benefits such as non-toxicity, instantaneous switching on and off, significantly longer lifetime, flexibility in the design of the reactor architecture and use of continuous current that allows direct connection with photovoltaic systems, [40,49,50], which together make them one of the most promising technologies for light assisted water disinfection processes.

5. Conclusions

This study has demonstrated the feasibility of using the UVC-LED assisted photo-Fenton process to achieve simultaneous water disinfection (including microorganisms resilient to UVC radiation) and CEC removal, meeting the EU 2020/741 standard for water reuse.

This comparison study showed that the treatment conditions which benefited disinfection hindered decontamination and vice versa. UVC light penetration in the reactor was found to have a predominant impact on disinfection and thus, the addition of Fe^{3+}-NTA hindered bacteria inactivation by reducing the UVC light delivered to the microorganisms. Conversely, decontamination was favoured by higher Fe^{3+}-NTA concentrations in the system, since it is the limiting reagent that governs kinetics of HO• generation through the photo-Fenton reaction. As a result of this compromise between both disinfection and decontamination, the oxidant H_2O_2 (1.47 mM) and Fe^{3+}-NTA (0.05 mM) at 30 min HRT allowed optimal conditions under continuous flow operation of the reactor, complying with the EU 2020/74 monitoring requirements, along with the simultaneous removal of microcontaminants. However, extended treatment times would be required to reach the EU 2020/741 validation target of ≥5 log-reduction for *C. perfringens*.

In summary, the results reported in this study have shed new light on the future implementation of the photo-Fenton process at neutral pH with low-energy artificial light which could also be powered by direct solar energy conversion in photovoltaics, for simultaneous wastewater disinfection and decontamination in batch and continuous flow reactors. However, further studies are still needed in terms of technology cost, efficiency, power output and process upscaling by coupling the kinetics with the radiation field inside reactor.

CRediT authorship contribution statement

T.B. Benzaquén: Writing – original draft, Methodology, Investigation, Formal analysis, Data curation, Conceptualization. **N. Pichel:** Writing – original draft, Methodology, Investigation, Formal analysis, Data curation, Conceptualization. **P. Soriano-Molina:** Writing – original draft, Methodology, Investigation, Formal analysis, Data curation, Conceptualization. **J.L. Casas López:** Writing – review & editing, Data curation, Project administration, Funding acquisition. **G. Li Puma:** Writing – review & editing, Conceptualization. **J.A. Sánchez Pérez:** Writing – review & editing, Supervision, Project administration, Funding acquisition, Conceptualization.

Declaration of competing interest

The authors declare that they have no known competing financial interests or personal relationships that could have appeared to influence the work reported in this paper.

Data availability

Data will be made available on request.

Acknowledgements

T.B. Benzaquén acknowledges funding from the Consejo Nacional de Investigaciones Científicas y Técnicas CONICET, Argentina. N. Pichel acknowledges funding from the Spanish Ministry of Economy and Competitiveness, 'Juan de la Cierva' Programme, Grant number FJC2019-042533-I. P. Soriano-Molina acknowledges the Andalusian Regional Government for her research contract (DOC_00544) funded by the ESF Operational Programme 2014–2020, community measure D1113102E3.

Funding

This work was supported by the project AT21-00204-UAL "Photoreactor for disinfection and removal of contaminants of emerging concern in treated wastewater" funded by the Consejería de Universidad, Investigación e Innovación de la Junta de Andalucía and the European Regional Development Fund, Operational Programme 2014–2020, the ANDROMEDA project (PID2022-140875OB-C31), the LIFE PHOENIX project, funded by the European Union under Grant Agreement No. LIFE19 ENV/ES/000278, and the PPIT-UAL, Junta de Andalucía-ERDF 2021–2027. Programme: 54.A.

Appendix A. Supplementary data

Supplementary data to this article can be found online at https://doi.org/10.1016/j.jwpe.2024.105518.

References

[1] Regulation (EU), 2020/741 of the European Parliament and of the Council of 15 May 2020 on minimum requirements for water reuse. Official Journal of the European Union. L 177/32, 5.6.2020. http://data.europa.eu/eli/reg/2020/741/oj.

[2] P. Krzeminski, M.C. Tomei, P. Karaolia, A. Langenhoff, C.M.A. Almeida, E. Felis, F. Gritten, H.R. Andersen, T. Fernandes, C.M. Manaia, L. Rizzo, D. Fatta-Kassinos, Performance of secondary wastewater treatment methods for the removal of contaminants of emerging concern implicated in crop uptake and antibiotic resistance spread: a review, Sci. Total Environ. 648 (2019) 1052–1081, https://doi.org/10.1016/j.scitotenv.2018.08.130.

[3] F.S. Mustafa, A.A. Oladipo, Photocatalytic degradation of metronidazole and bacteria disinfection activity of Ag-doped Ni0.5Zn0.5Fe2O4, J. Water Process eng. 42 (2021) 102132, https://doi.org/10.1016/j.jwpe.2021.102132.

[4] P.N. Patil, P.B. Managutti, A.F. Shunnar, B. Padmashali, A. Kumar, N. Kohli, V. Uppar, Synthesis of novel pyrrolo[1,2-a]quinoline derivates as a new class of anti-inflammatory and antimicrobial agents: an approach to single crystal X-ray structure, Hirshfeld surface analysis and DFT studies, J. Mol. Struct. 1296 (1) (2024) 136791.

[5] F.S. Mustafa, A.A. Oladipo, Dual function mg-doped binary metal ferrite: photocatalytic degradation of trichlorophenol, bactericidal activity and molecular docking analysis, Chemosphere 312 (2) (2023) 137348.

[6] A. De Luca, R.F. Dantas, S. Esplugas, Study of Fe(III)-NTA chelates stability for applicability in photo-Fenton at neutral pH, Catal. B: Environ. 179 (2015) 372–379, https://doi.org/10.1016/j.apcatb.2015.05.025.

[7] J.A. Sánchez Pérez, S. Arzate, P. Soriano-Molina, J.L. García Sánchez, J.L. Casas López, P. Plaza-Bolaños, Neutral or acidic pH for the removal of contaminants of emerging concern in wastewater by solar photo-Fenton? A techno-economic assessment of continuous raceway pond reactors, Sci. Total Environ. 736 (2020), https://doi.org/10.1016/j.scitotenv.2020.139681.

[8] G. Maniakova, I. Salmerón, M. Aliste, M.I. Polo-López, I. Oller, S. Malato, L. Rizzo, Solar photo-Fenton at circumneutral pH using Fe(III)-EDDS compared to ozonation for tertiary treatment of urban wastewater: contaminants of emerging concern removal and toxicity assessment *Chem*, Engl. J. 431 (4) (2022) 133474, https://doi.org/10.1016/j.cej.2021.133474.

[9] U.J. Ahile, R.A. Wuana, A.U. Itodo, R. Sha'Ato, R.F. Dantas, A review on the use of chelating agents as an alternative to promote photo-Fenton at neutral pH: current trends, knowledge gap and future studies, Sci. Total Environ. 710 (2020) 134872, https://doi.org/10.1016/j.scitotenv.2019.134872.

[10] Y. Zhang, N. Klamerth, P. Chelme-Ayala, M. Gamal El-Din. Comparison of Nitrilotriacetic Acid and [S,S]-Ethylenediamine-N,N′-disuccinic Acid in UV–Fenton for the Treatment of Oil Sands Process-Affected Water at Natural pH. Environ. Sci. Technol. 50 (2016) 10535–10544. doi:https://doi.org/10.1021/acs.est.6b03050.

[11] S. Wacławek, H.V. Lutze, K. Grübel, V.V.T. Padil, M. Černík, D.D. Dionysiou, Chemistry of persulfates in water and wastewater treatment: a review, Chem. Eng. J. 330 (2017) 44–62, https://doi.org/10.1016/j.cej.2017.07.132.

[12] J. Rodríguez-Chueca, S. Guerra-Rodríguez, J.M. Raez, M.J. López-Muñoz, E. Rodríguez, Appl. Catal. B Environ. 248 (2019) 54–61, https://doi.org/10.1016/j.apcatb.2019.02.003.

[13] H. Alamgholiloo, E. Asgari, S. Nazari, A. Sheikhmohammadi, N.N. Pesyan, B. Hashemzadeh, Assessment of different iron species as activators of S2O82- and HSO5- for inactivation of wild bacteria strains *Sep*, Purif. Technol. 300 (2022) 121911, https://doi.org/10.1016/j.seppur.2022.121911.

[14] C. Liu, L. Chen, D. Ding, T. Cai, Sulfate radical induced catalytic degradation of metolachlor: efficiency and mechanism, Chem. Eng. J. 368 (2019) 606–617, https://doi.org/10.1016/j.cej.2019.03.001.

[15] W. Ren, Z. Zhou, Y. Zhu, L. Jiang, H. Wei, T. Niu, P. Fu, Z. Qiu, Effect of sulfate radical oxidation on disintegration of waste activated sludge, Int. Biodeterior. Biodegradation 104 (2015) 384–390, https://doi.org/10.1016/j.ibiod.2015.07.008.

[16] A.C. Chevremont, A.M. Farnet, B. Coulomb, J.L. Boudenne, Effect of coupled UV-A and UV-C LEDs on both microbiological and chemical pollution of urban wastewaters *Sci*, Total Environ. 426 (2012) 304–310, https://doi.org/10.1016/j.scitotenv.2012.03.043.

[17] I. De la Obra, B. Esteban García, J.L. García Sánchez, Low cost UVA-LED as a radiation source for the photo-Fenton process: a new approach for micropollutant removal from urban wastewater *Photochem*, Photobiol. Sci. 16 (2017) 72–78, https://doi.org/10.1039/c6pp00245e.

[18] K. Song, M. Mohseni, F. Taghipour, Application of ultraviolet light-emitting diodes (UV-LEDs) for water disinfection: a review, Water Res. 94 (2016) 341–349, https://doi.org/10.1016/j.watres.2016.03.003.

[19] Y. Ahmed, J. Lu, Z. Yuan, P.L. Bond, J. Guo, Efficient inactivation of antibiotic resistant bacteria and antibiotic resistance genes by photo-Fenton process under visible LED light and neutral pH, Water Res. 179 (2020) 115878, https://doi.org/10.1016/j.watres.2020.115878.

[20] D.K. Kim, D.H. Kang, Efficacy of light-emitting diodes emitting 395, 405, 415, and 425 nm blue light for bacterial inactivation and the microbicidal mechanism, Food Res. Int. 141 (2021) 110105, https://doi.org/10.1016/j.foodres.2021.110105.

[21] I. Carra, J.A. Sánchez Pérez, S. Malato, O. Autin, B. Jefferson, P. Jarvis, Application of high intensity UVC-LED for the removal of acetamiprid with the photo-Fenton process, Chem. Eng. J. 264 (2015) 690–696, https://doi.org/10.1016/j.cej.2014.11.142.

[22] A. Cai, J. Deng, T. Zhu, C. Ye, J. Li, S. Zhou, Q. Li, X. Li, Enhanced oxidation of carbamazepine by UV-LED/persulfate and UV-LED/H2O2 processes in the presence of trace copper ions, Chem. Eng. J. 404 (2021) 127119, https://doi.org/10.1016/j.cej.2020.127119.

[23] N. López-Vinent, A. Cruz-Alcalde, C. Gutiérrez, P. Marco, J. Giménez, S. Esplugas, Micropollutant removal in real WW by photo-Fenton (circumneutral and acid pH) with BLB and LED lamps *Chem*, Engl. J. 379 (2020) 122416, https://doi.org/10.1016/j.cej.2019.122416.

[24] S. Miralles-Cuevas, I. De la Obra, E. Gualda-Alonso, P. Soriano-Molina, J.L. Casas López, J.A. Sánchez Pérez, Simultaneous disinfection and organic microcontaminant removal by UVC-LED-driven advanced oxidation processes, Water 13 (2021) 1507, https://doi.org/10.3390/w13111507.

[25] Watch List, https://www.legislation.gov.uk/eudn/2018/840/contents#.

[26] G.V. Buxton, A.J. Elliot, Rate constant for reaction of hydroxyl radicals with bicarbonate ions. International journal of radiation applications and instrumentation. Part C, Radiat. Phys. Chem. 27 (1986) 241–243, https://doi.org/10.1016/1359-0197(86)90059-7.

[27] S. Murov, I. Carmichael, G. Hug, Handbook of Photochemistry, second ed., Marcel Dekker, New York, 1993.

[28] Water quality – enumeration of Escherichia coli and coliform bacteria. Part 1: membrane filtration method for waters with low bacterial background flora, ISO 9308-1 (2014).

[29] Water quality – enumeration of Clostridium perfringens – method using membrane filtration, ISO 14189 (2017).

[30] H.E. Watson, Epidemiol. Infect. 8 (1908) 536–542, https://doi.org/10.1017/S0022172400015928.

[31] J.R. Bolton, K.G. Linden, Standardization of methods for Fluence (UV dose) determination in bench-scale UV experiments, J. Environ. Eng. 129 (3) (2003) 209–215, https://doi.org/10.1061/(ASCE)0733-9372(2003)129:3(209).

[32] A. Mejri, P. Soriano-Molina, S. Miralles-Cuevas, J.A. Sánchez Pérez, Fe3+-NTA as iron source for solar photo-Fenton at neutral pH in raceway pond reactors, Sci. Total Environ. 736 (2020) 139617, https://doi.org/10.1016/j.scitotenv.2020.139617.

[33] P. Prete, A. Fiorentino, L. Rizzo, A. Proto, R. Cucciniello, Open the way to turnover frequency determination in (photo)Fenton processes for catalytic activities comparison *Catal*, Today 424 (2022) 113864, https://doi.org/10.1016/j.cattod.2022.08.006.

[34] G. Li Puma, Modeling of thin-film slurry photocatalytic reactors affected by radiation scattering *environ*, Sci. Technol. 37 (2003) 783–5791, https://doi.org/10.1021/es0300362.

[35] R.E. Cantwell, R. Hofmann, M.R. Templeton, Interactions between humic matter and bacteria when disinfecting water with UV light, J. Appl. Microbiol. 105 (2008) 25–35, https://doi.org/10.1111/j.1365-2672.2007.03714.x.

[36] V. Baldasso, H. Lubarsky, N. Pichel, A. Turolla, M. Antonelli, M. Hincapie, L. Botero, F. Reygadas, A. Galdos-Berazategui, J.A. Byrne, P. Fernandez-Ibañez, UVC inactivation of MS2-phage in drinking water – modelling and field testing, Water Res. 203 (2021) 117496, https://doi.org/10.1016/j.watres.2021.117496.

[37] S. Belachqer-El Attar, P. Soriano-Molina, I. de la Obra, J.A. Sánchez Pérez, A new solar photo-Fenton strategy for wastewater reclamation based on simultaneous supply of H2O2 and NaOCl, Sci. Total Environ. 834 (2022) 155273, https://doi.org/10.1016/j.scitotenv.2022.155273.

[38] P. Soriano-Molina, I. De la Obra, S. Miralles-Cuevas, E. Gualda-Alonso, J.L. Casas López, J.A. Sánchez Pérez, Assessment of different iron sources for continuous flow solar photo-Fenton at neutral pH for sulfamethoxazole removal in actual MWWTP effluents, J. Water Process Eng. 42 (2021) 102109, https://doi.org/10.1016/j.jwpe.2021.102109.

[39] N. López-Vinent, A. Cruz-Alcalde, G. Gutiérrez, P. Marco, J. Giménez, S. Esplugas, Micropollutant removal in real WW by photo-Fenton (circumneutral and acid pH) with BLB and LED lamps, Chem. Eng. J. 379 (2020) 122416, https://doi.org/10.1016/j.cej.2019.122416.

[40] A. Kamel, M. Fuentes, A.M. Palacios, M.J. Rodrigo, M. Vivar, Deactivating environmental strains of Escherichia coli, *Enterococcus faecalis* and *Clostridium perfringens* from a real wastewater effluent using UV-LEDs. *Heliyon* 8 (12) (2022) e12628, https://doi.org/10.1016/j.heliyon.2022.e12628.

[41] T. Maezono, M. Tokumura, M. Sekine, Y. Kawase, Hydroxyl radical concentration profile in photo-Fenton oxidation process: generation and consumption of hydroxyl radicals during the discoloration of azo-dye Orange II, Chemosphere 82 (2011) 1422–1430, https://doi.org/10.1016/j.chemosphere.2010.11.052.

[42] C.J. Miller, A.L. Rose, T.D. Waite, Importance of Iron complexation for Fenton-mediated hydroxyl radical production at Circumneutral pH, Front. Mar. Sci. 3 (2016) 134, https://doi.org/10.3389/fmars.2016.00134.

[43] Y. Deng, R. Zhao, Advanced oxidation processes (AOPs) in wastewater treatment, Curr. Pollut. Rep. 1 (2015) 167–176, https://doi.org/10.1007/s40726-015-0015-z.

[44] S. Miralles-Cuevas, P. Soriano-Molina, I. de la Obra, E. Gualda-Alonso, J.A. Sánchez Pérez, Simultaneous bacterial inactivation and microcontaminant removal by solar photo-Fenton mediated by Fe^{3+}-NTA in WWTP secondary effluents, Water Res. 205 (2021) 117686, https://doi.org/10.1016/j.watres.2021.117686.

[45] K. Zhou, Z. Wang, X. Wang, G. Jiao, Y. Li, S.P. Sun, X.D. Chen, Degradation of emerging pharmaceutical micropollutants in municipal secondary effluents by low-pressure UVC-activated HSO5− and S2O82− AOPs, Chem. Eng. J. 393 (2020) 124712, https://doi.org/10.1016/j.cej.2020.124712.

[46] M. Eicher-Sodo, R. Gordon, Y. Zheng, Characterizing the phytotoxic effects of hydrogen peroxide on common microgreen species and lettuce cultivars, HortTechnology 29 (2019) 283–289, https://doi.org/10.21273/HORTTECH04255-18.

[47] I. De la Obra Jiménez, B. Esteban García, G. Rivas Ibáñez, J.L. Casas López, J. A. Sánchez Pérez, Continuous flow disinfection of WWTP secondary effluents by solar photo-Fenton at neutral pH in raceway pond reactors at pilot plant scale, Appl. Catal. B Environ. 247 (2019) 115–123, https://doi.org/10.1016/j.apcatb.2019.01.093.

[48] N. Pichel, H. Lubarsky, A. Afkhami, V. Baldasso, L. Botero, J. Salazar, M. Hincapie, J.A. Byrne, P. Fernandez-Ibañez, Safe drinking water for rural communities using a low-cost household system. Effects of water matrix and field testing, *J. Water Process.* Eng. 44 (2021) 102400, https://doi.org/10.1016/j.jwpe.2021.102400.

[49] J.R. Bolton, C.A. Cotton, The Ultraviolet Disinfection Handbook, American Water Works Association, 2008.

[50] B.S. Ritt, A.L.T. Fernande, G.T. Júnior, Comparative analysis between the chlorination and ultraviolet radiation methods for the disinfection of bacteria-contaminated water, Rev. Ambient. Água 16 (2021), https://doi.org/10.4136/ambi-agua.2654.